Tellus (2003), 55A, 338–351
Printed in UK. All rights reserved

TELLUS
ISSN 0280–6495

A numerical, high-resolution study of the life cycle of the severe storm over Denmark on 3 December 1999

By NIELS WOETMANN NIELSEN* and BENT HANSEN SASS, *Danish Meteorological Institute, Lyngbyvej 100, DK2100 Copenhagen Ø, Denmark*

(Manuscript received 4 February 2002; in final form 11 February 2003)

ABSTRACT

A severe cyclone with destructive effects moved across Denmark during the evening of 3 December 1999. A study, based on a numerical high-resolution limited area model simulation of this event, is presented. The development is of the frontal wave type. It can be interpreted qualitatively as an interaction between a PV wave at the tropopause, a surface temperature wave on the polar front and a low-level positive and upper-level negative PV anomaly generated by release of latent heat of condensation. In a run without this heat source the minimum sea level pressure in the cyclone increased from 954 to 978 hPa. As a result of the PV anomaly interactions the surface cyclone moves from the anticyclonic to the cyclonic shear side of the upper-level jet during its evolution from an incipient low to a mature cyclone. Its frontal structure evolves from an anticyclonic barotropic shear type to a barotropic type without shear. In the former state a low-level jet is confined to the warm sector of the surface cyclone. In the latter state a low-level bent-back front jet develops and becomes the most intense low-level jet. The time-scale from initiation to maximum intensity of the jet is about 9 h. The run without latent heat release develops similar, but weaker frontal structures, most notably a much weaker bent-back front.

1. Introduction

In Europe the weather in December 1999 was unusual in the sense that three very severe cyclones hit the continent on 3, 26 and 27 December, respectively (Ulbrich et al., 2001). The present paper deals with one of these storms. We made the obvious choice (from a national point of view) to study the cyclone on 3 December, because this cyclone went right across Denmark. It was such an extreme event that we name this cyclone the Denmark storm.

Most extratropical cyclones are predicted several days before they occur as a result of the great advances in numerical modeling and atmospheric data assimilation techniques. However, there are still developments which are not well predicted either due to deficiencies in atmospheric models or due to data assimilation shortcomings. Furthermore, a very accurate timing and intensity is sometimes required for specific purposes, e.g., in order to assess the risk of dangerous storm surge events in coastal areas. High accuracy in forecast skill would indeed have been required for the Denmark storm. The operational regional forecast model (Sass et al., 2000) at the Danish Meteorological Institute (DMI) did not meet the demands for exact timing and spatial distribution of the strongest surface winds required for accurate prediction of the water level along the North Sea coast of Jutland (56°N, 8°E). Moreover, the damage caused by this cyclone is considered to be the most severe for a hundred years or more. The maximum 10 min wind speed at 10 m height, measured at the west coast of Jutland, was about 38 m s^{-1} with 3 s gusts above 51 m s^{-1}.

The basic idea in the present paper is to study the development of the Denmark storm by using results from a numerical simulation instead of observations. This procedure appears to be justified because it is

*Corresponding author.
e-mail: nwn@dmi.dk

shown that the simulation of the storm compares well with observed key storm parameters such as path, central sea level pressure and intensity of the near-surface wind circulation. It is shown in section 2 that careful selection of the experimental system setup is essential to obtain a good simulation of the Denmark storm. The HIRLAM forecasting system is briefly described in Appendix A. Section 3 contains a validation of the predicted cyclone against observations. The result of the validation in section 3 is taken as sufficient justification for using a numerical simulation instead of observations in the study of the life cycle of the Denmark storm presented in section 4. This section also contains an investigation of how well the simulated storm fits conceptual models in extratropical cyclogenesis. Finally, section 5 contains discussion and conclusions.

2. Experimental system setup

The Danish Meteorological Institute High Resolution Limited Area Model forecasting system (DMI-HIRLAM) was run with access to less than the normal number of observations in the beginning of December 1999. The system made a fair prediction of the Denmark storm 48 h in advance, but at shorter forecast ranges, involving optimum interpolation analyses of the cyclone in its most rapidly deepening phase, the precision degraded somewhat and the predicted surface winds did not meet the operational requirements for accurate prediction of the sea level. Therefore, the study presented in section 4 is based on a re-run utilizing a revised forecasting system. Guidance from a number of experiments on the Denmark storm case was used to determine the architecture of the system setup for an improved numerical simulation of the severe cyclone. The experiments used 6 hourly analyses from the European Centre for Medium Range Weather Forecasts (ECMWF) for the lateral boundaries (with linear interpolation in time between the updates). Various runs were performed with different horizontal and vertical resolutions, with different sizes of the model domain, and with and without a number of 6 hourly adjustment steps. The possibility of making adjustment steps is a specific feature of DMI-HIRLAM. The adjustments are obtained from a first guess HIRLAM forecast field in high resolution, interpolated to a rotated ECMWF analysis grid point field. The difference between this interpolated field and the ECMWF analysis field is a kind of an analysis increment which is interpolated back to the high-resolution HIRLAM grid and added to the first guess value to produce the analysis state. The procedure allows for retaining small scales from the first-guess field in high resolution while incorporating the good quality of the large-scale ECMWF analyses.

The experimental system setup finally chosen for the numerical simulation of the Denmark storm is running with 50 vertical levels and a horizontal resolution of 0.15°. The model area covers a major part of Northern Europe and the North Atlantic Ocean. The number of horizontal grid points is 210×402. The geographical center of the model area is located west of the British Isles at 57°N, and 19°W. The dimensions of the area are approximately 3400 km in the north–south direction and 6400 km in the east–west direction. The lateral boundaries (with 6 hourly updates) are supplied by the ECMWF global model analyses with 60 vertical levels and a horizontal resolution of 0.5°.

The initial state of the simulation is achieved through a series of 6 hourly adjustment steps, as described above, making use of both the HIRLAM forecast model and ECMWF analyses. This method starts from an interpolated ECMWF analysis on 00 UTC 2 December 1999 with adjustment steps at 06 and 12 UTC followed by a 36 h forecast from the adjusted state at 12 UTC 2 December 1999.

3. Forecast versus observations

A major problem in studying marine extratropical cyclones is that very few observations are available along their tracks. Usually these cyclones pass over land areas with abundant observations in their mature or filling stages. Nevertheless, the progress in numerical weather prediction has reached a point where it has become possible to make fairly precise numerical simulations of marine extratropical cyclones, provided that their initial states have been analysed with sufficient accuracy. The realism of a numerical simulation of a cyclone evolution can be evaluated by observations if the cyclone track passes over regions with dense observations.

The Denmark storm is a good candidate for such a study, because it moved from the North Atlantic west of Ireland over the data-rich area of the United Kingdom in its most rapidly deepening phase and continued further eastward over Denmark in its mature stage.

In this section it is shown that the numerical simulation (with experiment name EGY) of the Denmark storm compares well with observed key parameters of

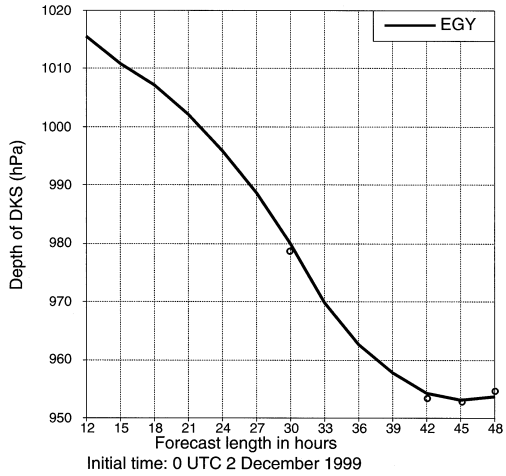

Fig. 1. Predicted central sea level pressure of the Denmark storm (DKS) as a function of forecast length (full curve) and observational estimates (open circles). The run starts from an initial time of 00 UTC 2 December 1999.

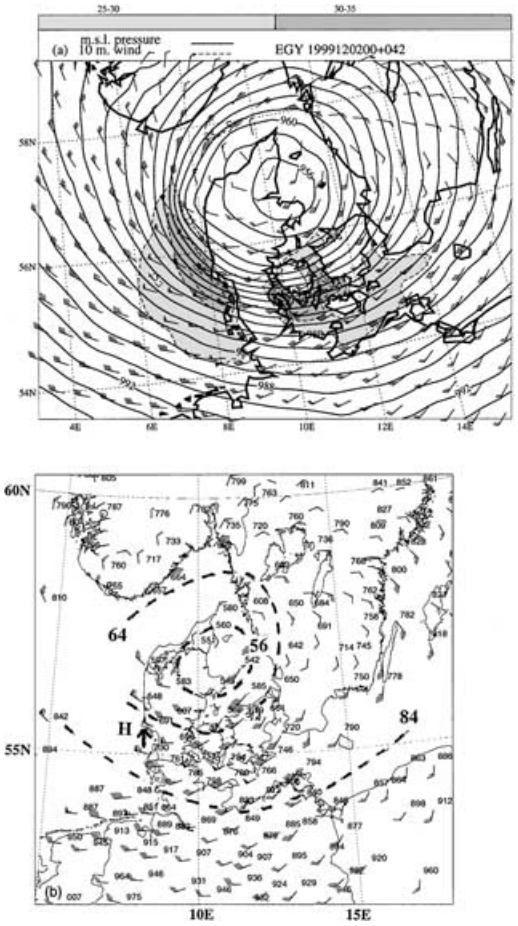

Fig. 2. (a) 42 h forecast of sea level pressure (full curves at 2 hPa intervals) and wind velocity (WMO standard) at 10 m height (dashed lines, contours 25, 30 and 32 m s^{-1}, light and dark shading for intervals 25–30 and 30–35 m s^{-1}, respectively) valid for 18 UTC 3 December. (b) Verifying observations on 18 UTC 3 December of sea level pressure and 10 m wind velocity (WMO standard). Dashed lines are subjectively analysed isobars at 956, 964 and 984 hPa. A vertical arrow (left) shows the position of Horns Rev (H).

this storm justifying the use of the simulation in a study of the evolution of the Denmark storm. A clear indication of the good quality of the simulation is given by Fig. 1, showing that the predicted depth of the storm (i.e. its central sea level pressure) is within a few hectopascals from the observed estimate. Note that no estimate is given in Fig. 1 at times where the density of observations makes reliable estimates difficult. The path and phase of the cyclone are also well predicted as indicated in Fig. 2. Note the flow across the center of the cyclone both in the forecast (Fig. 2a) and in the observations (Fig. 2b). This behavior can partly be explained by the isallobaric wind, which has a maximum in the core region of the sea level pressure system and is directed from west–southwest towards east–northeast (in the opposite direction of the horizontal gradient of the sea level pressure tendency).

The highest wind speeds recorded in Denmark in the 20th century were measured at the Wadden Sea coast of Jutland (near H in Fig. 2b) in connection with the Denmark storm around 18 UTC on 3 December 1999. We have used wind speed measurements from an off-shore tower in the Wadden Sea (position shown by H in Fig. 2b) to evaluate the predicted wind speeds in the simulation. The comparison is presented in Fig. 3. The observations are 10 min averaged wind speeds measured 30 m above sea level and the corresponding predicted values (interpolated to the tower position) are from model level 50 (approximately 35 m above sea level). The overall good correspondence between the observed and predicted curve is another confirmation of the reliability of the simulation.

4. The simulation of the storm

4.1. The cyclone development – an overwiev

According to the numerical simulation the Denmark storm initially formed between 06 and 12 UTC on 2 December 1999 as a col wave on a tight

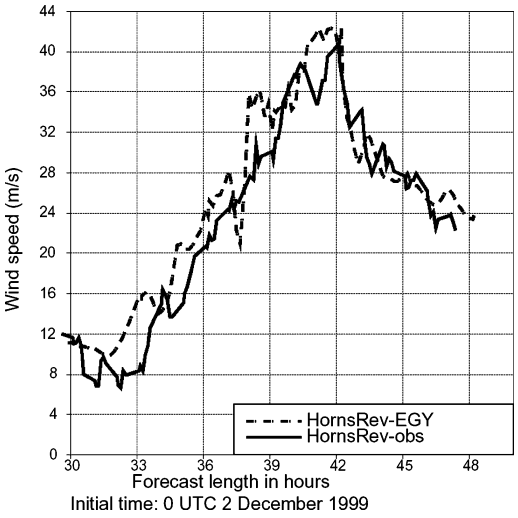

Fig. 3. Observed wind speed at 30 m height (full curve) and predicted wind speed at model level 50, at approximately 35 m height (dash-dotted curve). Observation and model output frequency of 10 m wind speed are every 10 and 12 min, respectively. Initial time of forecast as in Fig. 1.

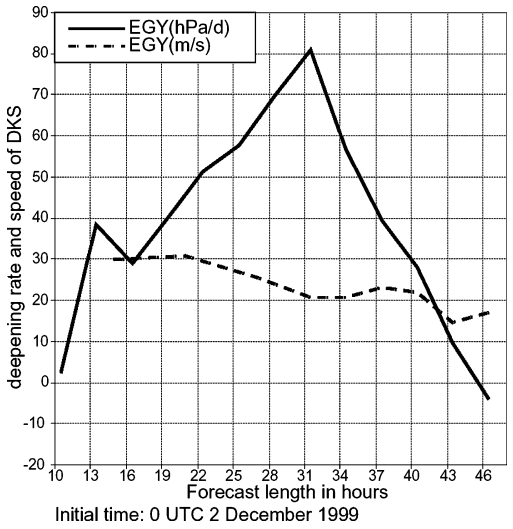

Fig. 4. Predicted deepening rate (hPa d^{-1}) and translation speed (m s^{-1}) of the Denmark storm (DKS) as a function of forecast length. Initial time of forecast as in Fig. 1.

lower-tropospheric polar front. At 12 UTC the incipient low was approximately at 52.5°N, 32.5°W, and 18 h later the fast moving low had entered its most rapidly deepening phase over Scotland. The mature stage was reached 12 h later (18 UTC on 3 December), while the center of the cyclone was over Denmark. At this stage of development the scale of the surface low (here estimated as twice the distance from the cyclone center to its outer closed isobar) was of the order of 1000 km. These observations classify the Denmark storm as a class 2 cyclone, according to a classification of extratropical cyclones proposed by Thorpe (1994). The variation in deepening rate and translation speed of the Denmark storm during its evolution is depicted in Fig. 4. The high maximum deepening rate (based on 3 hourly central sea level pressure) of about 80 hPa d^{-1} shows that the cyclone was of the 'bomb' type (Sanders and Gyakum, 1980). Similar high surface cyclone deepening rates have been reported over the eastern North Atlantic Ocean by e.g. Wernli (2002), Grønås et al. (1995) and Nielsen (1994).

Figure 5 summarises characteristic features of the cyclone evolution. It can be seen that the surface low forms on the equatorward, anticyclonic shear side of the jet stream (Fig. 5a) and moves east–northeastward during its development with the speed and deepening rates as shown in Fig. 4. The track of the surface low intersects the upper-level jet core, and it is seen that the deepening rate of the surface cyclone increases as its horizontal distance from the jet stream core decreases. The maximum deepening rate occurs in the period where the surface cyclone crosses beneath the jet stream core and emerges on its poleward, cyclonic shear side (Fig. 4 and Fig. 5b).

The configuration depicted in Fig. 5b is strikingly similar to the classical illustration of extratropical cyclogenesis shown in many textbooks on dynamic and synoptic meteorology (e.g. Bluestein, 1993). The position of the center of the surface low beneath the upper-level jet core between its trough and downstream ridge is favorable for the positive feedback between low-level warm advection and diabatic heating and upper-level positive vorticity advection, as confirmed by the peak deepening rate occuring in this period (Fig. 4).

Occasionally, jet streak dynamics, in particular the divergence in the left exit region of the jet streak, has been reported to play a significant role in extratropical cyclogenesis (e.g. Ucellini and Kocin, 1987). In the present case jet streak dynamics seems to play a secondary role for the development.

Extratropical cyclogenesis is frequently initiated as regions of significant positive vorticity advection associated with upper-level troughs and/or jet streaks approach low-level frontal zones. This common type

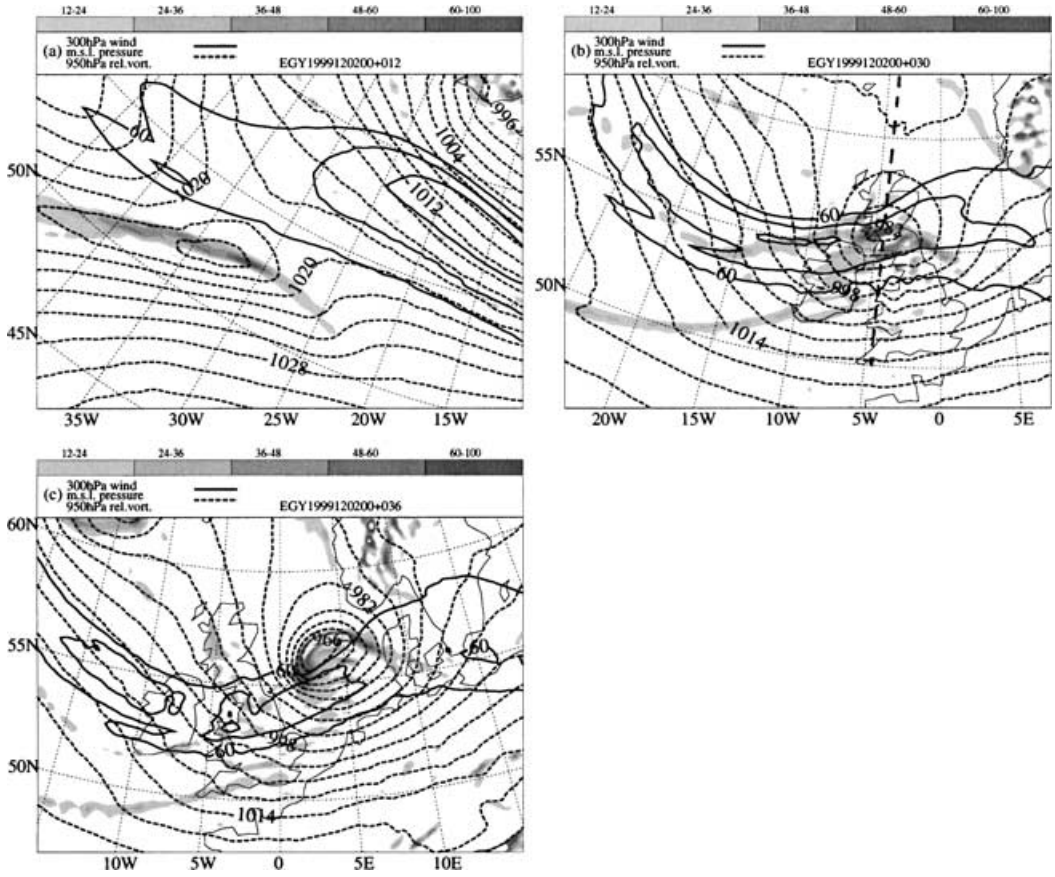

Fig. 5. Relative vorticity at 950 hPa $\geq 12 \times 10^{-5}$ s^{-1} (with shading intervals 12–24, 24–36, 36–48, 48–60, 60–100 and white $> 100 \times 10^{-5}$ s^{-1}), sea level pressure [dotted lines, contour interval 2 hPa in (a) and 4 hPa in (b) and (c)] and 300 hPa wind speed ≥ 60 m s^{-1} (full lines, contour interval 10 m s^{-1}). (a) is a 12 h forecast valid at 12 UTC 2 December, (b) is a 30 h forecast valid 06 UTC 3 December and (c) is a 36 h forecast valid at 12 UTC 3 December.

of cyclogenesis, involving positive feedback interaction between upper-level vorticity advection and low-level thermal advection and diabatic heating, is often called type B cyclogenesis (Petterssen and Smebye, 1971). In contrast, their type A cyclonesis is initiated by lower-tropospheric temperature advection and diabatic heating without any significant positive vorticity advection aloft. However, the latter source is gradually created by the type A self-development process.

The investigation shows that the Denmark storm has features in common with a type B development. First of all, the crossing tracks of the surface cyclone and the upper-level trough are a clear indication of their interation. To start with, the deepening of the surface cyclone is mainly due to warm advection and diabatic heating increasing with height above the surface low (figure not shown). Later in the development, upper-level vorticity advection becomes the main contributor to the deepening (Figs. 5b and 5c). The initial deepening due to warm advection and diabatic heating is not mentioned in the original definiton of a type B development.

4.2. The cyclogenesis from a potential vorticity perspective

It is instructive to discuss the cyclogenesis by using potential vorticity (PV) arguments. The indication in Fig. 4 of a local minimum in translation speed in the period of maximum deepening rates might be a result

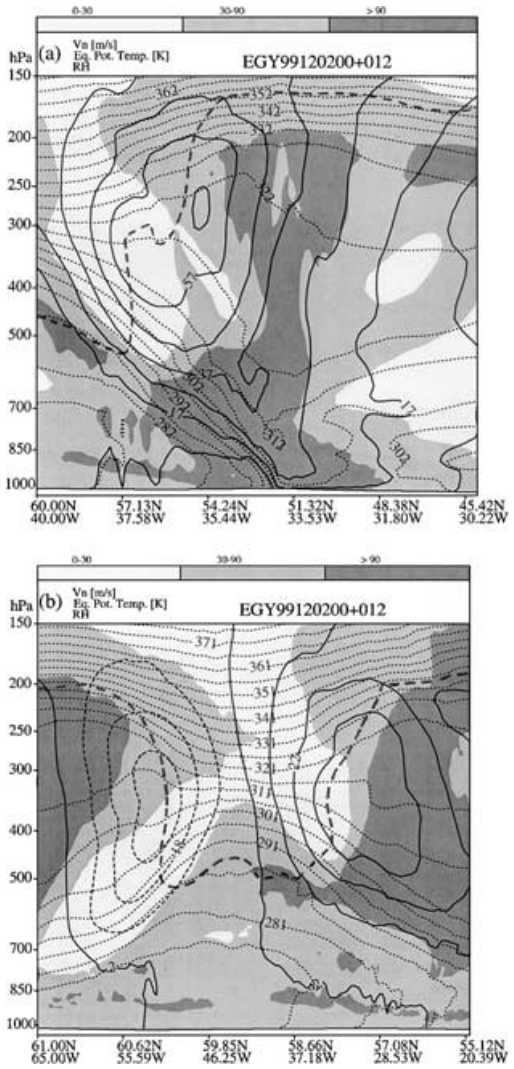

Fig. 6. Vertical cross-section with distribution of relative humidity RH (intervals 0–30, 30–70, 70–90 and above 90% with no, light, medium and dark shading, respectively), θ_e (dotted curves, contour interval 5 K) and wind speed V_n normal to the cross-section (full/dashed lines, contour interval 10 m s^{-1}). The thick dashed curve is the 1.5 PVU contour. (a) Cross-section along N–N′ in Fig. 7a; (b) cross-section along M–M′ in Fig. 7a. The forecast is valid at 12 UTC 2 December.

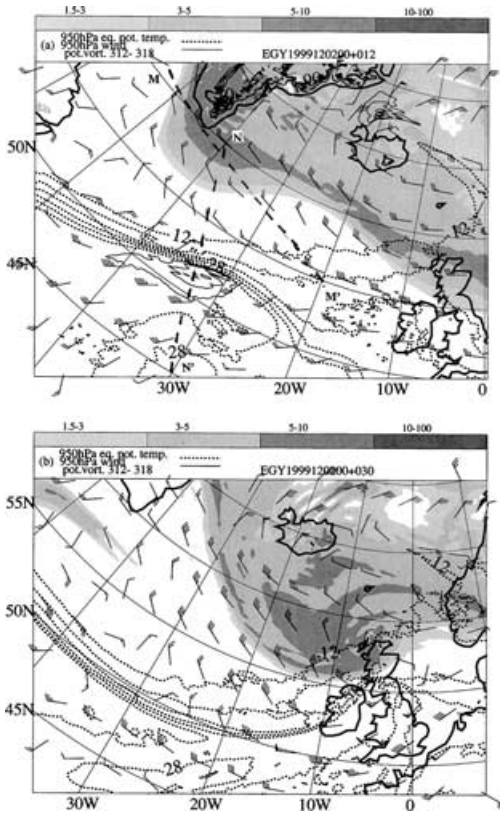

Fig. 7. Potential vorticity at 315 K ≥ 1.5 PVU (1 PVU = 10^{-6} m^2 s^{-1} K kg^{-1}) with shading intervals 1.5–3, 3–5, 5–10 and 10–100 PVU, θ_e at 950 hPa in interval 12–32 °C (dotted curves, contour interval 4 °C) and 950 hPa velocity (WMO standard). (a) 12 h forecast valid at 12 UTC 2 December and (b) 30 h forecast valid at 06 UTC 3 December. Full curves in (a) show 950 hPa wind speed ≥24 m s^{-1} at 3 m s^{-1} intervals and dashed lines N–N′ and M–M′ show the location of the vertical cross-sections in Figs. 6a and 6b, respectively.

of phase-locking (Hoskins et al., 1985) due to interaction between PV anomalies at the tropopause and at the surface. In the early stage of the cyclone development vertical cross-sections showing the lower- and upper-tropospheric PV anomalies are depicted in Figs. 6a and 6b, respectively. The horizontal separation of the PV anomalies is shown in Fig. 7. In the incipient stage of the surface cyclogenesis the two waves were more than 500 km apart in the meridional direction (Fig. 7a). The surface cyclone formed in a region of enhanced near-surface gradients of θ and θ_e. This is a region where the arctic and polar frontal zones merge. The jet cores associated with the frontal zones appear at 300 hPa as two separate wind maxima (Fig. 5a). A low-level jet formed in the warm and moist air on the equatorward side of the low-level frontal zone. Note that wind speeds around 30 m s^{-1} at 950 hPa occur in the inner part of the warm sector of the developing frontal wave.

As the surface cyclogenesis proceeds the surface cyclone and the upper-level jets come closer together, and at 06 UTC on 3 December (after less than 24 h of cyclogenesis) the surface cyclone, located at the ridge of the near-surface θ_e wave, has moved to a position at the outer edge and downstream of the axis of the cyclonic PV anomaly aloft (Fig. 7b). The deepening rate of the surface cyclone has increased to about 80 hPa d^{-1} (Fig. 4). The relative positions of the upper-level trough and the surface cyclone is as depicted in textbooks on baroclinic instability. The configuration shown in Fig. 7b together with low static stability promotes efficient positive feed back between upper-level cyclonic vorticity advection above the surface cyclone center and low-level cold and warm advection below the trough and the ridge, respectively, of the upper-level wave.

The interaction between the tropopause PV wave and the near-surface θ wave is illustrated in idealized form in Fig. 8. The circulation connected with the tropopause cyclonic PV anomaly brings the trough and ridge of the near-surface θ wave equatorward and poleward, respectively. Similarly, the circulation connected with the surface PV anomalies moves the trough and ridge of the tropopause PV wave, respectively, equatorward and poleward. The result is a mutual amplification of the waves, their PV anomalies and connected circulations. The wave amplification is illustrated in Fig. 8 by showing the waves at time t_1 and at a later time t_2. Note that we assumed that the relative translation speed of the waves was zero. The idealized development is qualitatively similar to the simulated development in Fig. 7. Note also that, because the tropopause PV wave propagates westward and the near-surface θ wave propagates eastward, the background westerly flow of the PV wave aloft must be considerably stronger than the low-level background flow of the near-surface θ wave to keep a zero relative translation speed.

It is clear from Fig. 8 that the PV anomalies can only interact if their connected circulations overlap in space. Figure 7a shows that the horizontal wave length λ of the waves is about 1800 km, while the horizontal and vertical separation of the waves is, respectively, about 0.3 λ and $h = 6$ km. The horizontal separation is close enough for overlap to take place between the horizontal projections of the circulations connected with the PV anomalies. The vertical penetration depth H is about $H = f\lambda/N$, where f is the Coriolis parameter and N is the Brunt–Väisälä frequency. This shows that also for high static stability the condition for interaction, i.e. $H > h$, is fulfilled. The investigation shows that the cyclonic tropopause PV anomaly and the sharp low-level frontal zone is present before any significant interaction takes place, but it has not been proven whether the near-surface θ wave is present prior to the period of interaction or it is triggered by the circulation connected with the cyclonic PV anomaly aloft.

The absence of a high-amplitude long-wave over the North Atlantic in the period of cyclogenesis is notable and gives room for a strong westerly jet stream with a length of about 2λ (Fig. 5a).

The role of diabatic heating has not been considered. In the quasi-geostrophic framework its effect is similar to the effect of warm advection. Diabatic heating may play a significant role in the development of the Denmark storm right from its incipient stage. It is in fact possible that a localized diabatic heating maximum generated in the ascending branch of the frontal circulation (Eliassen, 1962) forms the incipient surface low and initiates low-level temperature advection. Its effect would also be, in line with warm advection, to amplify the upper-level ridge in Fig. 8. As discussed by Dixon et al. (2002) it is possible that moist symmetric

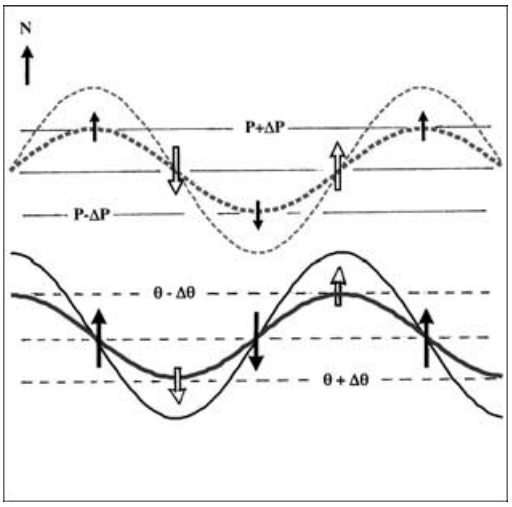

Fig. 8. Schematic representation of the interaction between a tropopause PV anomaly (thick and thin dashed curves at times t_1 and $t_2 > t_1$, repectively) and a surface θ anomaly to the south (thick and thin full curves at times t_1 and $t_1 > t_1$, repectively). A zonal backgroud PV field at tropopause level is shown by full lines, and the corresponding surface θ field is shown by zonal dashed lines. Open and full arrows indicate the circulation connected with the tropopause PV anomaly and the surface θ anomaly, respectively.

instability (MSI) enhances the atmospheric response to frontogenesis in this early phase of development. In the present study we have not investigated MSI. Neither has the impact on the cyclogenesis of diabatically generated low-level and upper-level positive and negative PV anomalies, respectively, been directly assessed. However, in a simulation of the Denmark storm without latent heat release its deepening was about 40%, less, with an increase to 978 hPa in minimum sea level pressure. A similar percentage has been reported for another intense East Atlantic winter storm by Grønås (1995). The experiments show that although release of latent heat is not necessary for this type of cyclogenesis, it is essential for capturing the intensity of the developing cyclone. It appears to be by far the most important diabatic heat source. In comparison, sensitivity tests on the Denmark storm case showed that sensible and latent heat flux at the air–sea interface had very little impact on the cyclogenesis. The radiative effect on the evolution has not been investigated.

4.3. Evolution of frontal structure

The influence of the barotropic shear in the planetary-scale flow on extratropical cyclogenesis has been studied in idealized numerical simulations (e.g. Hoskins and West, 1979; Simmons and Hoskins, 1979; Hoskins, 1990; Davies et al., 1991; Thorncroft et al., 1993; Wernli, 1995; Methven, 1996). In these studies three types of barotropic shear have been considered: the non-shear barotropic case, referred to as Life Cycle 1 (LC1), the cyclonic barotropic shear case (Life Cycle 2; LC2) and the anticyclonic barotropic shear case (Life Cycle 3; LC3). Recent studies by Shapiro et al. (1999), indicate that barotropic shear in the planetary-scale environmental flow of the real atmosphere (with all its complexity retained) also has an impact on the evolution of real extratropical cyclones and their frontal structures.

The present study showed that the time evolution of the low-level frontal structure of the Denmark storm was closely linked to the position of the center of the surface cyclone relative to the upper-level jet core. The frontal structure changed from LC3 to LC1 characteristics during the life cycle of the cyclone.

In phase 1, which is the open wave stage, the Denmark storm was situated on the anticyclonic shear side of the upper-level polar/arctic jet. Its frontal structure (Fig. 5a) showed similarity with the idealized anticyclonic barotropic shear case (LC3) in Wernli (1995), and with the development of the second secondary wave (Low 39a of FASTEX IOP-15) in Shapiro et al. (1999).

Phase 2 had a surface frontal fracture. Formation of the fracture was in progress in the period in which the surface cyclone center crossed beneath the upper-level jet core (Figs. 5b, 9a, 9b and 10a). The formation of the frontal fracture has been discussed by Browning et al. (1997). Their analysis showed that the formation of the frontal fracture (and an associated over-running dry intrusion) was related to the descent of an upper-level maximum of PV within a developing tropopause fold. Figure 9a, representing the early stage of frontal fracture formation, shows that dry air is present above a moist bottom layer on the equatorward side of the low-level frontal zone. In the frontal fracture zone the moist air is overrun by lower θ_e air (indicated by an open arrow in Fig. 9a). The over-running low θ_e air can be identified with the leading edge of colder air that in the storm-relative system advances eastward to the south of the surface cyclone center. As in the case studied by Browning et al. (1997), the process creates in the fracture zone a potentially unstable layer from about 700 to 900 hPa.

The dry air (or dry intrusion) on the warm side of the upper-level front has been advected around the base of the upper-level trough. It originates from levels near the tropopause and has a similar origin as the dry air mass poleward of the upper-level jet in Fig. 6a. The vertical humidity distribution in the cyclone area, depicted in Fig. 9a, is verified by soundings over the British Isles (e.g. Boulmer at 55.41°N, 1.60°W and Hillsborough at 54.48°N, 6.10°W) at 5 UTC on 3 December (not shown). The dry intrusion is also visible in the satellite image, shown in Fig. 11a.

At the time of Fig. 9a it is likely that the secondary circulation associated with upper-level frontogenesis advects fresh dry air from near-tropopause levels downward in the upper-level frontal zone in a tropopause folding process, originally described by Reed (1955) and Danielsen (1964). The presence of a sharp upper-tropospheric frontal zone during this period of development is in Fig. 9a shown by closely spaced θ_e-contours together with a strong vertical shear of the cross-section normal wind. Note the vertical alignment and separation of the tropopause-based and surface-based frontal zones. This configuration, occurring in the period of maximum deepening of the surface cyclone, is optimal for a vertically coupled upper- and lower-tropospheric jet-front system [Fig. 2.105 in Bluestein (1993), reproduced from Shapiro (1982)].

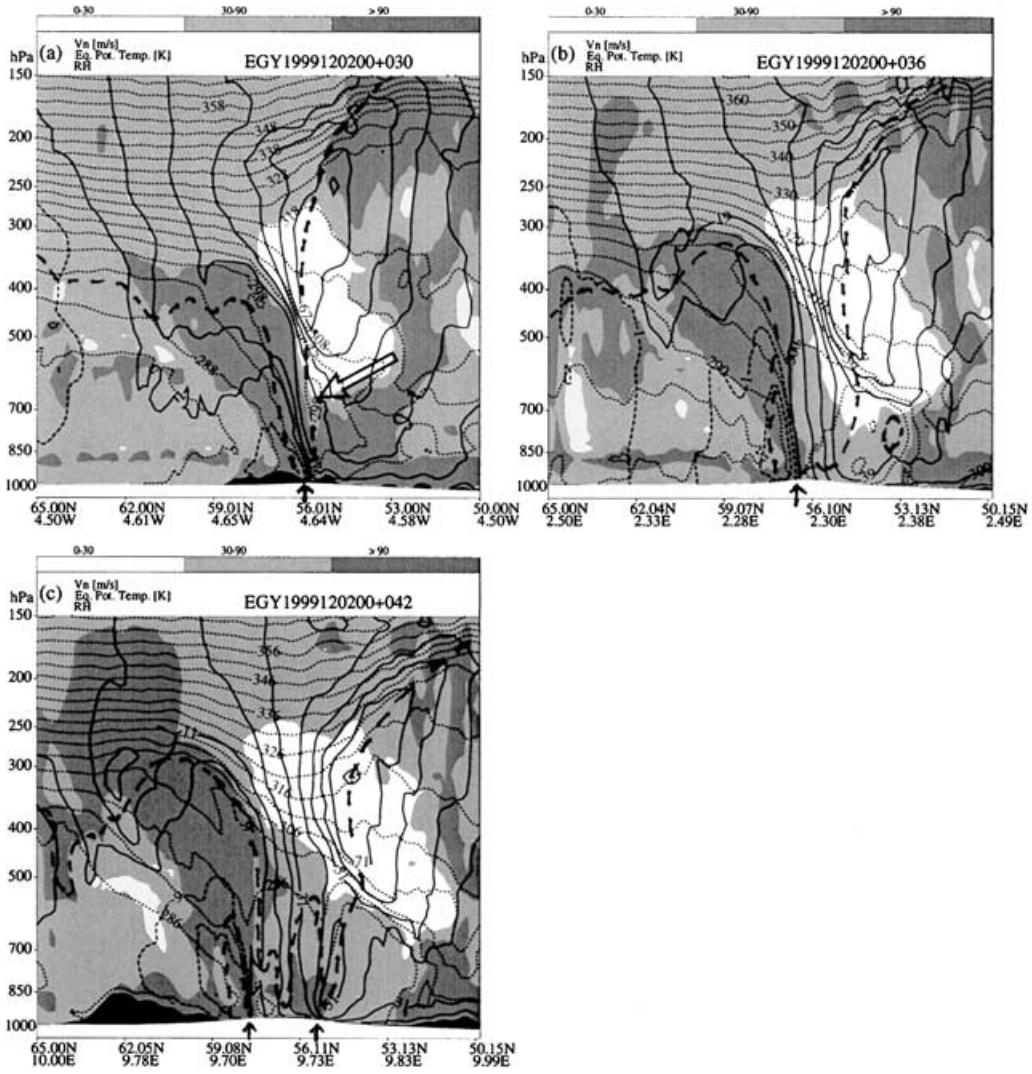

Fig. 9. Vertical cross-section with relative humidity RH (intervals 0–30, 30–70, 70–90 and above 90% with no, light, medium and dark shading, respectively), θ_e (dotted curves, contour interval 5 K) and wind speed V_n normal to the cross-section (full lines, contour interval 10 m s^{-1}). The thick dashed curve is the 1.5 PVU contour. (a) Cross-section valid at 06 UTC 3 December, approximately at 4.5°W, along the dashed line in Fig. 5b. (b) Cross-section valid at 12 UTC 3 December, approximately at 2.5°E, along the dashed line in Fig. 10a. (c) Cross-section valid at 18 UTC 3 December, approximately at 10.0° E, along the dashed line in Fig. 10b. Black arrows show the position of the surface bent-back front. The open arrow in (a) points to a region of potential instability.

The most spectacular change in the frontal structure occured in phases 3 and 4. During this stage of cyclogenesis the surface low moved from beneath the upper-level jet core to its cyclonic (and cold) shear side. The continued deepening was mainly due to differential vorticity advection above the center of the surface cyclone.

In phase 3 the cyclone developed a T-bone structure (Shapiro and Keyser, 1990) with a cold front nearly perpendicular to the warm front and a bent-back front

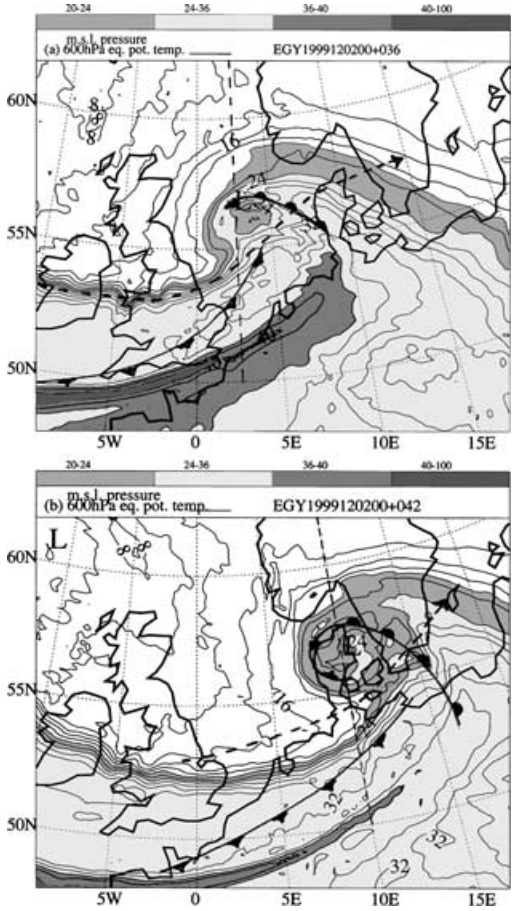

Fig. 10. Distribution of θ_e in °C at 600 hPa (full lines, contour interval 2 °C with medium, light, dark and very dark shading of the intervals 20–24, 24–36, 36–40 and 40–100 °C, respectively). Surface fronts are shown with conventional symbols, the center of the surface low is marked by L and the jet core at 300 hPa is shown by a thick dashed curve with and arrow showing the flow direction. (a) 36 h forecast valid at 12 UTC 3 December and (b) 42 h forecast valid at 18 UTC 3 December. The thin dashed lines show approximately the location of the vertical cross-sections in Figs. 9b and 9c.

continuing in the warm front poleward and ahead of the fracture (Fig. 10a). According to Shapiro et al. (1999) the T-bone frontal structure is typical for a LC1 development approaching maximum intensity. The LC1 case in Shapiro et al. (1999) has a vertical alignment of the subtropical and polar jets. The case under investigation here was similar in the sense that the polar and arctic jets in the region of cyclogenesis had become unified (Fig. 9). In the T-bone phase the bent-back front rapidly evolved backward with respect to the surface cyclone center.

In phase 4 the surface cyclone continued its movement away from the jet core deeper into the cold air. The evolving bent-back front began to encircle the cyclone center and finally cut off a pocket of relatively warmer air at the cyclone center. In this warm core seclusion phase part of the bent-back front south of the surface cyclone center was running nearly parallel with the upper-level jet core below its cyclonic shear side (Figs. 9c and 10b). Phase 4 was further characterized by a rapid decline in deepening rate.

The run without latent heat release also developed the T-bone and warm core seclusion features, but the sharpness of the bent-back front was weaker. The trailing cold front was on the other hand sharper in the run without latent heat release (figure not shown).

4.4. Evolution of low-level jets

Figure 7 shows that in phases 1 and 2 of the development of the Denmark storm the strongest near-surface winds occured in its warm sector. The warm sector low-level jet is linked to the warm near-surface θ anomaly at the warm side of the low-level frontal zone. The anomaly is equivalent to a cyclonic (positive) PV anomaly concentrated at the surface (Bretherton, 1966).

The above situation prevailed in the open-wave stage of the cyclone evolution. However, the situation changed rapidly from the moment the bent-back front began to form. A low-level jet associated with the warm θ anomaly at the bent-back front developed in response to the frontogenesis. The low-level enhanced cyclonic PV at the bent-back front is shown in Figs. 9b and 9c. The cyclonically sheared circulation associated with and centered on the positive low-level PV anomaly generates a low-level jet on the outer side of the PV anomaly and weakens the cyclonic flow on the opposite side of the anomaly. In this phase of the development high precipitation rates occured in the bent-back frontal zone, increasing from less than 1 mm h^{-1} at its rear end to about 8 mm h^{-1} near the cold frontal fracture zone (figure not shown). This indicates that the low-level positive PV anomaly was mainly generated by a maximum in latent heat release in the ascending branch of the bent-back frontal circulation. This is supported by the predicted 12 h accumulated precipitation until 18 UTC on 3 December. Its maximum values between 28 and 33 mm $(12\ h)^{-1}$ in a band located 50–150 km

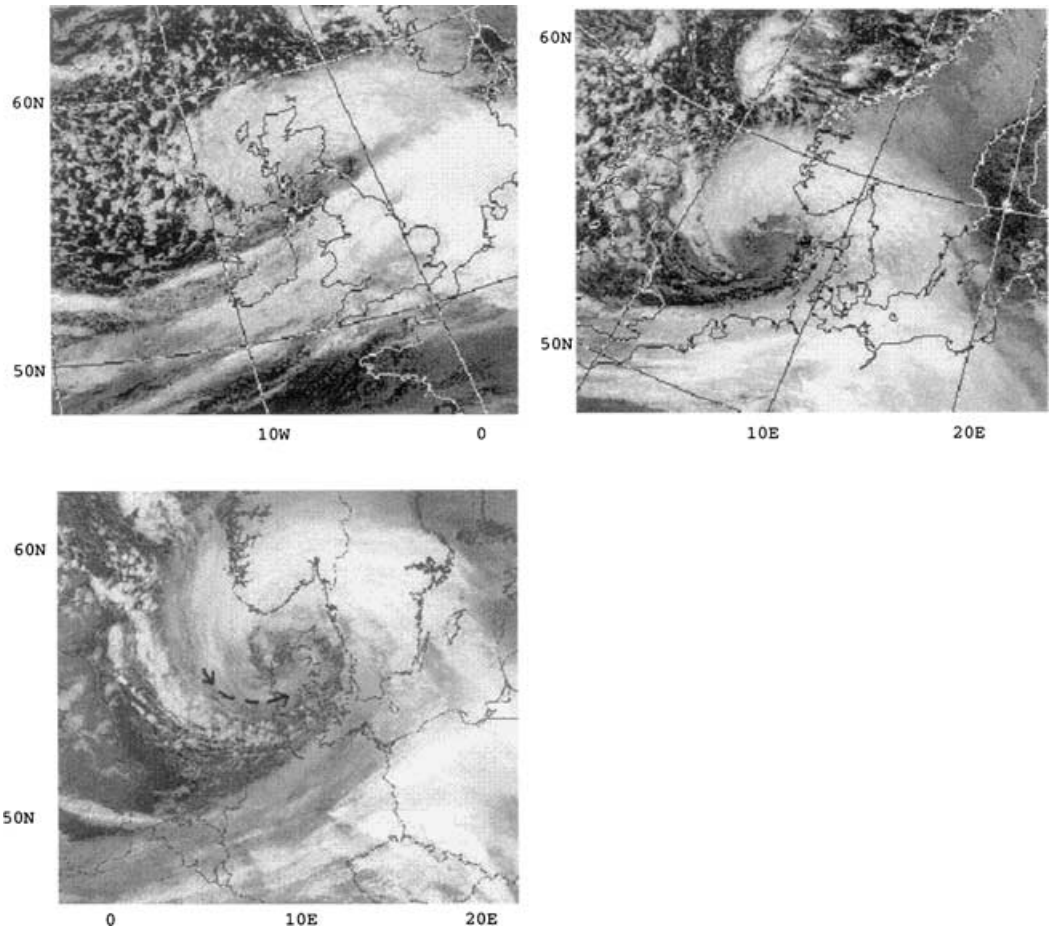

Fig. 11. NOAA infrared satellite images at (a) 05:36 UTC 3 December, (b) 13:52 UTC 3 December and (c) 17:49 UTC 3 December. In (c) the dashed curve with arrows indicates the position and flow direction of the low-level jet BBJ (see text).

poleward of the track of the center of the surface cyclone is within the range of observed maximum amounts (figure not shown). The mechanism appears to be similar to that forming a strongly convex cloud head in the 23 December 1997 cyclone described in Dixon et al. (2002).

The evolution of the low-level jets in the warm air and in connection with the bent-back front from the frontal fracture to the warm core seclusion phase is shown schematically in Fig. 12. This figure also shows the position of the upper-level jet core relative to the low-level jets. According to Fig. 12 the bent-back front jet (BBJ) becomes the dominating low-level jet in the transition period between the frontal fracture and the T-bone phase. The figure also shows the intensification with time of the BBJ in response to the continued deepening of the cyclone. Another property of the BBJ is its downstream intensification, which seems to be related to a more favorable downstream superposition of the circulations connected with the bent-back front PV anomaly and the (considerably lowered) tropopause and tropopause fold PV anomaly (Figs. 9c and 10b). The rapid development of the BBJ is a particularly important forecasting aspect. Note that the BBJ forms and develops to maximum intensity within 9 h.

The cloud-producing rising motion of the frontal circulation visualize the bent-back front in satellite images. For the Denmark storm this is shown, for example, by the similarity between the low-level θ_e and

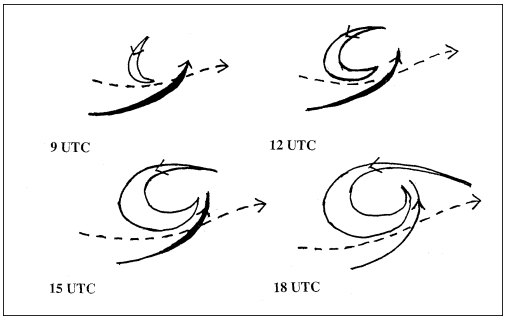

Fig. 12. Conceptual model of the evolution of the low-level jet (BBJ) associated with the bent-back front from the frontal fracture (9 UTC), over the T-bone (12 UTC) to the warm core seclusion phase (15 and 18 UTC). Full arrow, low-level jet in the warm air; open arrow, the BBJ and dashed arrow, jet core at 300 hPa. Arrow thickness of the low-level jets is proportional to wind speed. The states marked by 12 UTC and 18 UTC correspond to the observed states in Fig. 11b and Figs. 2b and 11c, respectively.

PV patterns (figures not shown) and the cloud head in Figs. 11a and 11b. The resemblance between the low-level θ_e and PV pattern and the cloud pattern of the cyclone continues into the seclusion phase (Fig. 11c). According to the analysis above, the BBJ blows with maximum strength near the outer edge of the cyclone's comma-shaped cloud head. This is confirmed by comparing the wind observations in Fig. 2b with the satellite image in Fig. 11c. In the latter figure the location of the BBJ is shown by a dashed curve with arrows indicating the flow direction.

5. Conclusions

We have investigated the development of a severe storm over Denmark from its early stages on 2 December 1999 over the central North Atlantic Ocean to its mature stage over southern Scandinavia on 3 December 1999. The study, supported by observations, shows that the development is of the frontal wave type, i.e. with a relatively small horizontal scale of the order 1000 km and a 1–2 d timescale. The evolution can be interpreted qualitatively as an interaction between a PV wave at the tropopause and a surface θ wave on the polar front combined with a low-level positive and upper-level negative PV anomaly generated by release of latent heat of condensation. The impact of latent heat release has been assessed indirectly by performing a run without this heat source. In the latter simulation the surface cyclone deepened to 978 hPa as compared to 954 hPa in the simulation with latent heat release. This indicates that low-level positive PV anomalies and upper-level negative PV anomalies generated by localized maxima in release of latent heat take very active part in the cyclogenesis.

As a result of the PV anomaly interactions the surface cyclone moves from the anticyclonic to the cyclonic shear side of the upper-level jet during its evolution from an incipient low to a mature cyclone. In the early stages of development warm advection and diabatic heating plays an important role for the deepening of the surface cyclone. In the later stages positive vorticity advection aloft becomes the main forcing term. The movement of the surface cyclone relative to the upper-level jet has important consequences for the development of frontal structures and their associated low-level jets. In the open-wave stage the surface cyclone is situated on the anticyclonic shear side of the upper-level jet core, and its frontal structure shows similarity with the idealized anticyclonic barotropic shear case (LC3) in Wernli (1995). The low-level jet is confined to the warm sector in this phase of development. As the surface cyclone emerges on the cyclonic shear side of the upper-level jet core its frontal structure changes rapidly and shows similarity with the non-shear barotropic (LC1) case. A bent-back front low-level jet develops on a 9 h timescale and becomes the dominating low-level jet. In a description of the development of the surface cyclone the Shapiro–Keyser frontal-cyclone life cycle model (Shapiro and Keyser, 1990) and Browning's conceptual air stream model (Browning, 1990) appear to be valuable extensions to the Bergen School Model (Bjerknes, 1919; Bjerknes and Solberg, 1922; Godske et al., 1957) for the type of very intense cyclogenesis presented. Other cyclone developments, particularly those of type LC2, may follow the Bergen School Model more closely (Shapiro et al., 1999). The run without latent heat release develops similar, but weaker frontal structures, most notably a much weaker bent-back front.

Guidance from a number of experiments on the Denmark storm case was used to determine how the system should be set up for an improved numerical simulation of the severe cyclone. A good initial state was obtained by making two adjustment steps involving ECMWF analyses. It was found that both a high horizontal and vertical resolution (0.15° and 50 levels, respectively) was needed to meet the demands for high accuracy forecasting of both the track and phase

of the cyclone and the intensity of the low-level jet that developed in its mature phase. In addition it was important that the model domain was chosen so large that it contained the entire path of the cyclone from its incipient stage to its mature stage. An almost equally good result was obtained on a smaller model domain, not containing the early part of the cyclone track, if the lateral boundaries were updated every third hour instead of every sixth hour (with linear interpolation in time between the updates).

In the present study the evolution of the Denmark storm has been described qualitatively. A quantitative study of very intense extratropical cyclogenesis to investigate in depth the role of various physical processes, including moist symmetric instability, remains to be done. The Denmark storm appears to be a good candidate for such a study, first of all because of the good observation coverage along its track from the United Kingdom to southern Sweden, and secondly because of the successful simulation of this cyclone.

6. Acknowledgements

We thank J. U. Jørgensen, DMI, for assistance in preparing the experimental system setup and H.S. Christensen, ELTRA, for supplying wind data from Horns Rev.

7. Appendix

A numerical weather prediction system (DMI-HIRLAM) is used in the present study. This forecasting system is used operationally at the Danish Meteorological Institute (DMI). HIRLAM stands for HIgh Resolution Limited Area Model, which implies that the model integrations are made for a limited area with lateral boundary conditions supplied by a host model, in this case from the ECMWF model. The DMI forecasting system originates from the international HIRLAM project. This collaboration started in 1985 and has continued since then. The national meteorological institutes of Sweden, Spain, Norway, Ireland, Iceland, Holland, Finland and Denmark participate in the development of the forecasting system. A documentation of the DMI-HIRLAM forecasting system is available (Sass et al., 2000). Here we outline the characteristics of the forecasting system.

The numerical model is a hydrostatic grid point model. The dynamical primitive equations are solved for a general pressure-based and terrain-following coordinate system. The atmospheric forecast variables are the horizontal wind components and surface pressure, temperature, specific humidity, specific cloud condensate and subgrid scale kinetic energy.

The dynamics are of Eulerian type using second-order accurate finite differences. The lateral boundary conditions are given by a host model (analyses or forecasts). All the key physical processes are included, i.e. the parameterizations of radiation, stratiform condensation, convection, turbulence and surface processes.

The dynamics and the physical parameterizations are coupled in such a way that the physics runs with longer time steps than used in the dynamics (Sass et al., 2000). The tendencies of the model variables from the dynamics required by the turbulence and convection parameterization are averaged in time. This strategy reduces numerical noise associated with interaction between dynamics and physics, and it enables reasonably long time steps in the physics to be retained at a high model resolution.

A fast radiation scheme developed for high-resolution meso-scale models (Savijärvi, 1990) has been adopted. The scheme for parameterizing cloud effects has been developed further for HIRLAM purposes.

The turbulence scheme (Cuxart et al., 2000) includes a treatment of 'subgrid scale kinetic energy' as a prognostic variable. Currently no 'gravity wave drag' scheme is used. Frictional effects are expressed in terms of an effective roughness parameter only.

The operational convection scheme is based on a moisture convergence closure and is viewed as a further development of the ideas of Kuo (1974). The moisture convergence includes the effect of surface evaporation flux. The convection parameterization describes vertical redistribution of moisture, cloud condensate and heat. The microphysics related to the condensation and precipitation processes follow rather closely the comprehensive treatment of Sundqvist (1993).

Surface fluxes are computed in a traditional framework involving drag formulae. The surface flux valid for a grid square is a weighted average of fluxes valid for land, ice and sea, respectively. Special attention is paid to the flux parameteriation over sea. Individual roughness lengths are applied for momentum, heat and moisture, respectively. As the wind speed goes towards zero in unstable conditions a treatment of 'free convection' assures that the surface fluxes are maintained at a reasonable magnitude.

REFERENCES

Bjerknes, J. 1919. On the structure of moving cyclones. *Geofys. Publ.* **1**, 1–8.

Bjerknes, J. and Solberg, H. 1922. Life cycle of cyclones and the polar front theory of atmospheric circulation. *Geofys. Publ.* **3**, 1–18.

Bluestein, H. B. 1993. *Synoptic–dynamic meteorology in midlatitudes, Vol. 2. Observations and theory of weather systems*. Oxford University Press, Oxford.

Bretherton, F. P. 1966. Critical layer instability in baroclinic flows. *Quart. J. R. Meteorol. Soc.* **92**, 325–334.

Browning, K. A. 1990. Organization of clouds and precipitation in extratropical cyclones. In *Extratropical cyclones: the Eric Palmén memorial volume*. (eds. C. W. Newton and E. O. Holopainen) Am. Meteor. Soc., Washington, D.C. 129–153.

Browning, K.A., Ballard, S. and Davitt, C. 1997. High-resolution analysis of frontal structure. *Mon. Wea. Rev.* **125**, 1212–1230.

Cuxart, J., Bougeault, P. and Redelsperger, J.-L. 2000. A turbulence scheme allowing for meso-scale and large-eddy simulations. *Quart. J. R. Meteorol. Soc.* **126**, 1–30.

Danielsen, E. F. 1964. Project springfield report. In *Defence Atomic Support Agency, DASA 1517,* 97 pp.

Davies, H., Schær, C. and Wernli, H. 1991. The palette of fronts and cyclones within a baroclinic wave-development. *J. Atmos. Sci.* **48**, 1666–1689.

Dixon, R. S., Browning, K. A., and Shutts, G. J. 2002. The relation of moist symmetric instability and upper-level potential-vorticity anomalies to the observed evolution of cloud heads. *Quart. J. R. Meteorol. Soc.* **128**, 839–860.

Eliassen, A. 1962. On the vertical circulation in frontal zones., *Geofys. Publ.* **24**, 147–169.

Godske, C. L., Bergeron, T., Bjerknes, J. and Bundgaard, R. 1957. *Dynamic meteorology and weather forecasting*. Am. Meteorol. Soc. and Carnegie Institute, Washington, D.C.

Grønås, S. 1995. The seclusion intensification of the new year's day storm 1992. *Tellus* **47A**, 733–746.

Hoskins, B. J. 1990. Theory of extratropical cyclones. In *Extratropical cyclones: the Eric Palmén memorial volume*. (eds. C. W. Newton and E. O. Holopainin) Am. Meteorol. Soc., Washington, D.C. 63–80.

Hoskins, B. J. and West, N. V. 1979. Baroclinic waves and frontogenesis. part ii: Uniform potential vorticity jet flows-cold and warm fronts. *J. Atmos. Sci.* **36**, 1663–1680.

Hoskins, B. J., McIntyre, M. E. and Robertson, A. W. 1985. On the use and significance of isentropic potential vorticity maps. *Quart. J. R. Meteorol. Soc.* **111**, 877–946.

Kuo, H. L. 1974. Further studies of the parameterization of the influence of cumulus convection on large-scale flow. *J. Atmos. Sci.* **3**, 1232–1240.

Methven, J. 1996. Tracer behaviour in baroclinic waves. Ph.D. Thesis, Reading University, U.K.

Nielsen, N. W. 1994. The 915-hPa cyclone of 10 January 1993. In *The life cycles of extratropical cyclones, Vol. 2*. (eds. S. Grønås and M. A. Shapiro) Am. Meteorol. Soc., Washington, D.C. 301–306.

Petterssen, S. and Smebye, S. J. 1971. On the development of extratropical cyclones. *Quart. J. R. Meteorol. Soc.* **97**, 457–482.

Reed, R. J. 1955. A study of a characteristic type of upper level frontogenesis. *J. Meteorol.* **12**, 226–237.

Sanders, F. and Gyakum, J. R. 1980. Synoptic–dynamic climatology of the 'bomb'. *Mon. Wea. Rev.* **108**, 1589–1606.

Sass, B. H., Nielsen, N. W., Jørgensen, J. U., Amstrup, B. and Kmit, M. 2000. The operational HIRLAM system at DMI. DMI Tech. Rep. No. 00-26, Danish Meteorological Institute, Copenhagen, Denmark.

Savijärvi, H. 1990. Fast radiation parameterization schemes for mesoscale and short-range forecast models. *J. Appl. Meteorol.* **29**, 437–447.

Shapiro, M. A. 1982. Mesoscale weather systems of the central united states. In *CIRES* University of Colo./NOAA, Boulder, Colorado.

Shapiro, M. A. and Keyser, D. 1990. Fronts, jet streams and the tropopause. In *Extratropical cyclones: the Eric Palmén memorial volume*. (eds. C. W. Newton and E. O. Holopainin) Am. Meteorol. Soc., Washington, D.C. 167–191.

Shapiro, M., Wernli, H., Bao, J.-W., Methven, J., Zou, X., Doyle, J., Holt, T., Grell, E. and Neiman, P. 1999. A planetary-scale to mesoscale perspective of the life cycles of extratropical cyclones: The bridge between theory and observations. In *The life cycles of extratropical cyclonesis*. (eds. S. Grønås and M. A. Shapiro) Am. Meteorol. Soc., Washington, D.C. 139–185.

Simmons, A. and Hoskins, B.J. 1979. Barotropic influences on the growth and decay of nonlinear baroclinic waves. *J. Atmos. Sci.* **37**, 1679–1684.

Sundqvist, H. 1993. Inclusion of ice phase of hydrometeors in cloud parameterization for mesoscale and largescale models. *Beitr. Phys. Atmosph./Contrib. Atmos. Phys.* **66**, 137–147.

Thorncroft, C., Hoskins, B. J. and McIntyre, M. E. 1993. Two paradigms of baroclinic-wave life cycle behavior. *Quart. J. R. Meteorol. Soc.* **119**, 17–55.

Thorpe, A. J. 1994. Dynamics of mesoscale sub-structure of fronts. In *The life cycles of extratropical cyclones*, *Vol. 1*. (eds. S. Grønås and M.A. Shapiro) Am. Meteorol. Soc., Washington D.C. 220–228.

Ucellini, L. W. and Kocin, P. J. 1987. The interaction of jet-streak circulations during heavy snow events along the East Coast of the United States. *Wea. Forecasting* **1**, 289–308.

Ulbrich, U., Fink, A. H., Klawa, M. and Pinto, J. G. 2001. Three extreme storms over Europe in December 1999., *Weather* **56**, 70–80.

Wernli H., Durren S., Lininger M. A. and Zelly, M. 2002. Dynamical aspects of the life cycle of the winter storm 'Lothar' (24–26 December 1999). *Quart. J. R. Meteorol. Soc.* **128**, 405–430.

Wernli, J. H. 1995. Lagrangian perspective of extratropical cyclogenesis. Dissertation no. 11016, Swiss Federal Institute of Technology (ETH), Zurich, Switzerland.